https://doi.org/10.5194/egusphere-2026-2316
Preprint. Discussion started: 8 May 2026

Light availability controls multi-decadal trends in crustose coralline algal cell elongation

Bastian Seidl[1], Ines Pyko[1], Thomas Mölg[2], Wendy Nelson[3,4], Sebastian Teichert[1]

[1]GeoZentrum Nordbayern, Lehrstuhl für Paläoumwelt, Friedrich-Alexander-Universität Erlangen-Nürnberg (FAU), Loewenichstraße 28, 91054 Erlangen, Germany
[2]Climate System Research Group, Institute of Geography, Friedrich-Alexander-Universität Erlangen-Nürnberg (FAU), Wetterkreuz 15, 91058 Erlangen, Germany
[3]Herbarium, Natural Sciences Department, Tāmaki Paenga Hira Auckland Museum, Auckland Domain, Auckland, New Zealand
[4]School of Biological Sciences, University of Auckland, Auckland, New Zealand

Correspondence to: (bastian.seidl@fau.de)

Abstract. Crustose coralline algae (CCA) are globally distributed calcifying macroalgae that can grow as free-living rhodoliths, act as ecosystem engineers by creating complex three-dimensional habitats, and contribute to the carbon cycle. The dimensions of cells in the carbonate skeleton influence rhodolith structural integrity and, consequently, the ecological functions these rhodoliths provide, yet CCA cellular responses to environmental change remain poorly resolved. This study quantifies multi-decadal variability in skeletal cell dimensions of the rhodolith-forming CCA *Sporolithon nodosum* from New Zealand and evaluates the relative importance of sea surface radiation (SSR), sea surface temperature (SST) and sea surface CO_2 partial pressure (pCO_2) as potential drivers. The length and width of 2975 cells were measured along a 38-year transect (1985–2022) using stitched scanning electron microscope images. Cell length declined significantly over time (R^2_{adj} = 0.105, p = 0.027), whereas cell width showed no temporal trend (R^2_{adj} = -0.019, p = 0.583). Among the environmental variables, SSR was the strongest predictor of cell length (R^2_{adj} = 0.235, p = 0.001), while SST and pCO_2 explained comparatively little variance. These results identify light availability as a primary correlate of cell elongation in *S. nodosum*, consistent with a role for irradiance-driven changes in photosynthetic energy supply. Because long-term SSR trends are spatially heterogeneous, light-mediated shifts in CCA cell dimensions – and their potential implications for rhodolith structure and ecosystem function – are likely to vary regionally. This study highlights the central role of light availability in shaping CCA cell morphology under changing surface-ocean conditions and motivates multi-site comparisons to assess broader ecosystem implications.

1 Introduction

Crustose coralline algae (CCA) are heavily calcifying macroalgae that occur from tropical (Caragnano et al., 2016) to polar latitudes (Wisshak et al., 2017; López Correa et al., 2023), and across a broad bathymetric range from the intertidal zone (Basso et al., 2009) to depths reaching 268 m (Littler et al., 1985). Although most species are marine, some species colonise freshwater

https://doi.org/10.5194/egusphere-2026-2316
Preprint. Discussion started: 8 May 2026

habitats (Žuljević et al., 2016; Ragazzola et al., 2020). Because of their calcification, CCA have an excellent fossil record and stem groups of recent taxa are probably rooted in the Paleozoic (Granier, 2016; Teichert et al., 2019). These algae grow either attached to fixed substrates or as free-living nodules, referred to as rhodoliths when the CCA skeleton comprises more than 50% of the structure's volume (Bosence, 1983; Pyko et al., 2025). CCA fulfil a wide range of ecosystem functions, providing complex three-dimensional habitats such as rhodolith beds (Rebelo et al., 2022; Cabrito et al., 2024; Straube et al., 2024) and enhancing the structural stability of coral reefs (Teichert et al., 2020a; Cornwall et al., 2023). They also contribute to the carbon cycle through high rates of carbon uptake and substantial deposition of $CaCO_3$ (Schubert et al., 2024; Teichert, 2024) as well as the production and storage of floridean starch (Teichert, 2013; Gabsteiger et al., 2025).

CCA precipitate a high-Mg calcite skeleton (Smith et al., 2012), with growth increments characterised by an apparent alternation of longer, thin-walled and shorter, thick-walled cells (Basso, 1994; Basso et al., 1997; Kamenos and Law, 2010; Burdett et al., 2011; Caragnano et al., 2016; Bracchi et al., 2021). These growth increments are generally interpreted as annual (Freiwald and Henrich, 1994), which allows each increment to be assigned to a specific year of formation, although potential sub-annual banding has also been observed (Sletten et al., 2017). Annual growth rates do not decline with increasing specimen age, demonstrating the absence of an ontogenetic trend (Adey, 1964; Halfar et al., 2008). The algal thallus is anatomically differentiated into an epithallus composed of the outer cell layers, a perithallus forming the main algal body and a hypothallus containing the basal layers (Woelkerling, 1988; Irvine and Chamberlain, 1994). Adjacent cell lumina may be interconnected by primary and secondary pit connections (Auer and Piller, 2020; Pueschel, 2021; McCoy et al., 2023), which potentially facilitate intercellular transport (Kim et al., 2022; McCoy et al., 2023). During growth, new cells are formed in an intercalary meristem located between the epithallus and perithallus (Adey, 1964). Calcification of the carbonate skeleton begins in the middle lamella between adjacent cells (Vesk and Borowitzka, 1984; de Carvalho et al., 2017; McCoy et al., 2023), and subsequently progresses into the cell walls on both sides of the middle lamella (de Carvalho et al., 2017; McCoy et al., 2023). Whether this calcification process is biologically induced (de Carvalho et al., 2017; Nash et al., 2019) or actively controlled by the algae (Borowitzka, 1984; Cabioch and Giraud, 1986; Bracchi et al., 2021) remains unresolved.

Previous studies show that environmental variables such as light availability, temperature and CO_2 strongly influence the growth rate (Halfar et al., 2011; Williams et al., 2018; Teichert et al., 2024), carbonate production (Burdett et al., 2011; Martin et al., 2013; Teichert and Freiwald, 2014) and the geochemical composition of the carbonate skeleton (Ragazzola et al., 2016; Williams et al., 2018; Teichert et al., 2020b). This environmental sensitivity forms the basis for the widespread use of CCA as proxies in reconstructions of temperature (Halfar et al., 2000; Kamenos et al., 2008; Hetzinger et al., 2009; Gamboa et al., 2010; Darrenougue et al., 2014; Williams et al., 2014; Fietzke et al., 2015; Caragnano et al., 2017), sea ice variability (Halfar et al., 2013; Chan et al., 2017; Hetzinger et al., 2019; Leclerc et al., 2024), seawater pH (Fietzke et al., 2015) and anthropogenic pollution (Darrenougue et al., 2018).

Although the effects of environmental variables on growth rate, carbonate production and geochemical composition of CCA have been widely studied, comparatively little is known about their influence on cell dimensions. Nevertheless, the length and width of cells, together with cell wall thickness, play a key role in determining the structural integrity of rhodoliths (Ragazzola

https://doi.org/10.5194/egusphere-2026-2316
Preprint. Discussion started: 8 May 2026

et al., 2012; Melbourne et al., 2023). Understanding how environmental drivers influence CCA cell dimensions is therefore essential for assessing how ongoing anthropogenic climate change may affect these ecosystem engineers and their key roles in rhodolith beds, coral reef stabilisation, and the carbon cycle.

Existing studies provide valuable but fragmented insights into this issue. In laboratory experiments, Ragazzola et al. (2012) exposed rhodoliths consisting of the CCA *Boreolithothamnion glaciale* (Kjellman) Gabrielson, Maneveldt, Hughey & Peña to CO_2 above ambient levels. This resulted in longer, wider cells with thinner walls after three months (Ragazzola et al., 2012), although the effect was not sustained over longer experimental timescales (Ragazzola et al., 2013). Similarly, Melbourne et al. (2023) measured 25 ± 10 cells per sample from summer growth increments and reported increased lumen length and width in contemporary rhodoliths compared to specimens collected in the 1900s. These differences were primarily attributed to long-term warming and acidification (Melbourne et al., 2023). Bracchi et al. (2021) measured ten cells per sample across rhodoliths collected from different water depths and observed a decrease in cell length with depth, while cell width remained unchanged. Given the exponential attenuation of light with depth (Kirk, 2011) and the light-dependence of photosynthetic activity (Baek et al., 2022), this decline in cell length may reflect reduced energy availability at greater water depths. Although these studies collectively indicate that light availability, temperature and CO_2 affect cell dimensions, it remains unclear which variable exerts the strongest long-term control.

The present study quantifies the long-term effects of sea surface radiation (SSR), sea surface temperature (SST) and sea surface CO_2 partial pressure (pCO_2) on cell dimensions within a rhodolith mainly formed by the CCA *Sporolithon nodosum* Farr & Nelson from the Whangaparāoa Peninsula, New Zealand. It is hypothesised that cell length is positively correlated with SSR, consistent with the light-dependence of photosynthetic activity (Baek et al., 2022) and depth-related trends (Bracchi et al., 2021), with weaker influences of SST and pCO_2. Cell width is expected to show comparatively limited variation in response to environmental changes, as indicated by depth-related observations (Bracchi et al., 2021). Data were obtained by measuring the length and width of 2975 cells along a transect spanning 38 years (1985–2022) using stitched scanning electron microscope (SEM) images. Temporal trends in mean annual length and width were assessed using linear regression, while multiple linear regression with stepwise model selection was used to evaluate the impact of environmental parameters.

2 Methods

2.1 Sample collection

Living rhodoliths were collected in March 2023 from the shallow rocky subtidal zone at Army Bay (36°35′56.05″ S 174°48′47.45″ E) on Whangaparāoa Peninsula (Fig. 1a–c). The Whangaparāoa Peninsula extends approximately 12 km east–west into the Hauraki Gulf, north of Auckland on the North Island of New Zealand. Samples were obtained by snorkelling at depths of 1–5 m, and subsequently air-dried prior to further processing.

https://doi.org/10.5194/egusphere-2026-2316
Preprint. Discussion started: 8 May 2026

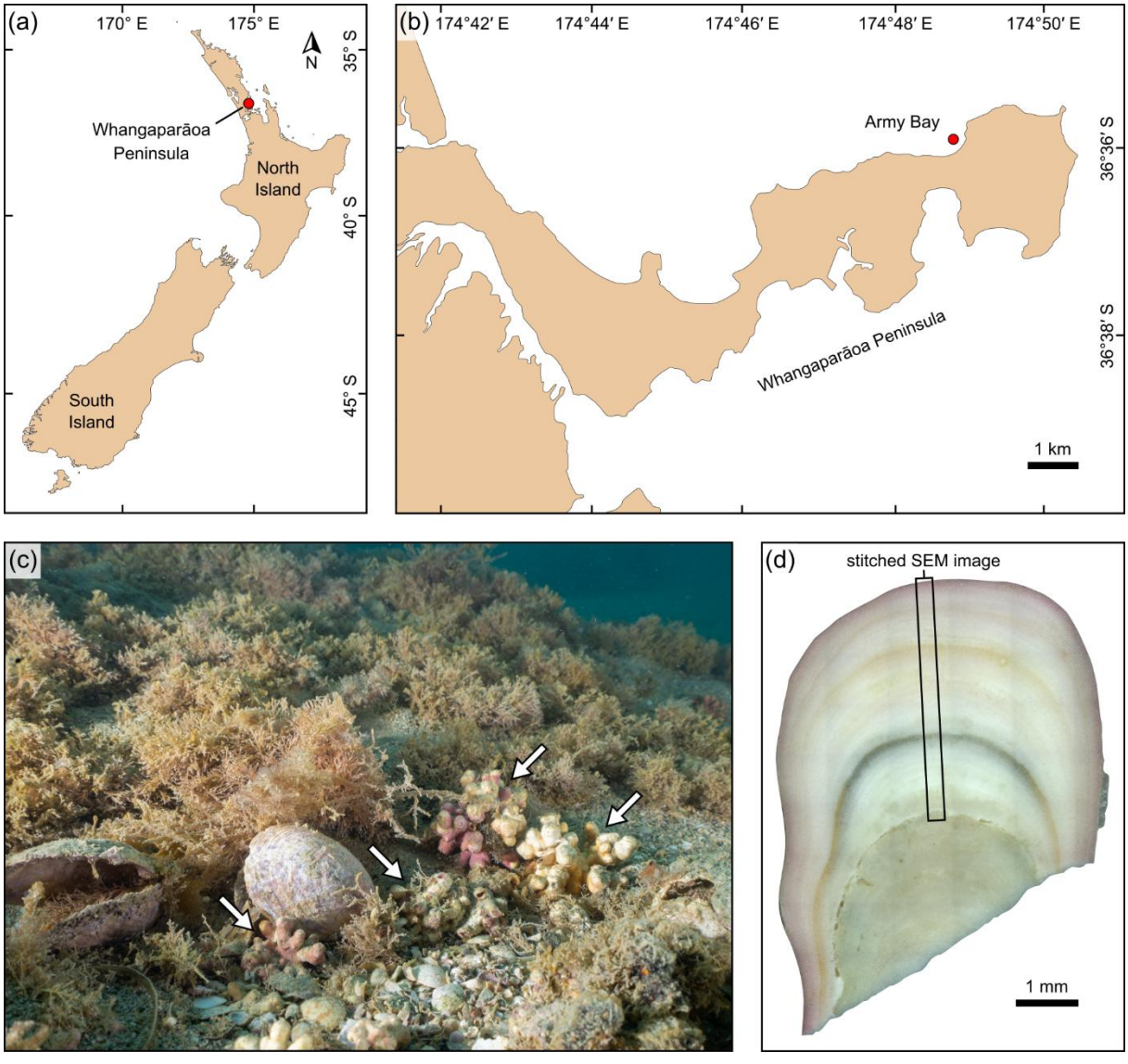

Figure 1. Overview of the study area and analysed protuberance. **(a)** Location of the Whangaparāoa Peninsula, New Zealand. **(b)** Sampling location in Army Bay on the Whangaparāoa Peninsula (36°35′56.05″ S 174°48′47.45″ E). **(c)** Rhodoliths in the shallow subtidal zone at Army Bay, indicated by white arrows, alongside brown algae and shell fragments. Image courtesy of Peter Marriott. **(d)** Longitudinal section through the analysed protuberance, used to establish the chronology of growth increments and showing the position of the stitched scanning electron microscope image used for cell measurements.

https://doi.org/10.5194/egusphere-2026-2316
Preprint. Discussion started: 8 May 2026

2.2 Sample preparation

Precise control of cell orientation is essential for accurately measuring three-dimensional features in two-dimensional sections (Bracchi et al., 2021). To account for variability in cutting orientation, five protuberances from different live-collected rhodoliths were prepared for SEM analysis following the procedure outlined below. From these, one protuberance with the most regular alignment of cells relative to the image plane was selected for detailed quantitative analysis, thereby minimising measurement biases associated with tilted cells.

Initially, all five protuberances were removed from their respective rhodoliths using pliers, embedded in epoxy resin (Biresin®), and cured for 72 h at 30 °C. The samples were then cut longitudinally with a Mecatome T180 water-cooled diamond rock saw, polished with 800-grit SiC powder and cleaned in an ultrasonic bath of demineralised water for 2 min to remove any residual grinding material. To enhance the visible relief between the middle lamella and the adjacent cell walls, samples were etched with 10 % acetic acid for 30 seconds and ultrasonicated in demineralised water for a further 10 min. Finally, the samples were mounted on aluminium stubs using epoxy resin and sputter coated with gold in a Cressington 108auto sputter coater operated at 10 kV and 30 µA for three cycles of 2 min each. Imaging was performed using a TESCAN Vega.xmu SEM with an SE detector at an acceleration voltage of 20 kV.

2.3 Cell dimension measurements

To quantify cell dimensions in the selected protuberance, SEM images were captured along a transect perpendicular to the growth increments (Fig. 1d). Because rhodoliths are free-living and may be periodically rotated, growth can be interrupted when parts of the thallus face downward or become buried in sediment for extended periods (Wilson et al., 2004). Such interruptions may lead to the formation of a growth hiatus (Schlüter et al., 2021), evidenced by localised cell death, which disrupts the continuity of growth increments (Wilson et al., 2004). To avoid biases in assigning years to growth increments, analyses were therefore restricted to growth increments above the first hiatus, where chronological control is reliable.

Images at 2000× magnification were arranged in a grid of 2 columns and 45 rows, with approximately 20% overlap between adjacent tiles to facilitate stitching (Fig. 2a). Stitching was performed using the *Grid/Collection Stitching* Plugin (Preibisch et al., 2009) in *Fiji* (Schindelin et al., 2012; version 2.16.0), employing linear blending to generate a seamless composite image. The resulting image measured approximately 285 µm in width and 4130 µm in height and spans from the epithallus to the first hiatus (Fig. 3a).

Cell length and width were manually measured in *Fiji* using the line tool, with a custom-written macro used to assign a unique identifier to each cell and overlay measurement lines and labels onto the image for visual verification. Spatial coordinates within the stitched SEM image were recorded for each measurement. Length measurements were taken along the longitudinal axis between opposing middle lamellae, while width was recorded perpendicular to this axis (Fig. 2b, c). In instances where the middle lamella between cells was damaged or obstructed, measurements were inferred from adjacent cells, provided that a clear grid pattern was present. If damage was too extensive for reliable inference, adjacent cells within the same row were

https://doi.org/10.5194/egusphere-2026-2316
Preprint. Discussion started: 8 May 2026

measured instead. A minimum of 10 cells per row were measured between the epithallus and the top of the hypothallus over a
130 transect of approximately 180 µm by 3900 µm (Fig. 3a).

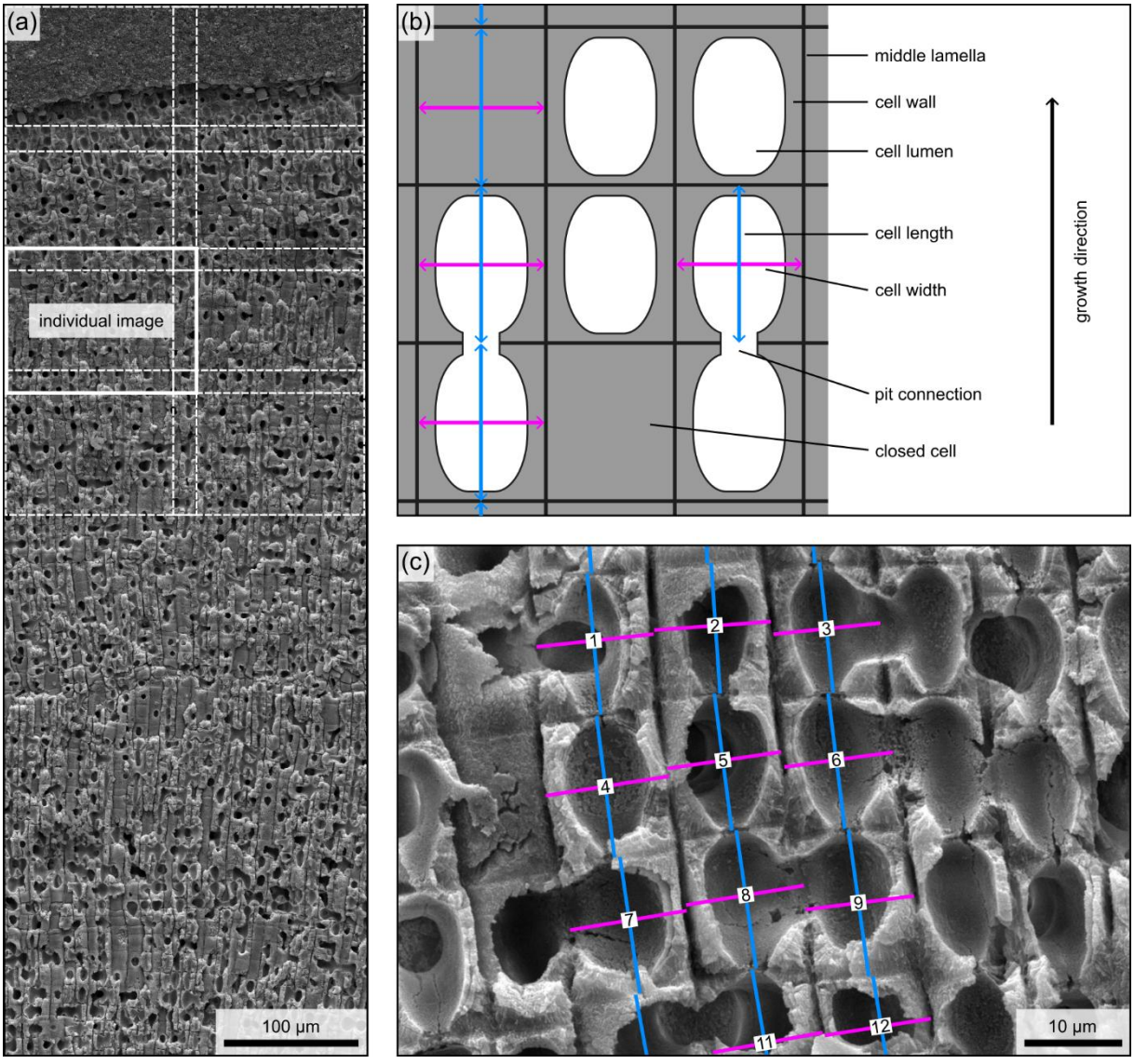

Figure 2. Methodology for image acquisition and measurements. **(a)** Upper portion of the stitched SEM image, with dotted lines indicating the boundaries and overlap of individual images. **(b)** Schematic depicting the terminology used to describe cell morphology and the corresponding measurements. **(c)** SEM image illustrating the application of measurements across three cell columns.

https://doi.org/10.5194/egusphere-2026-2316
Preprint. Discussion started: 8 May 2026

2.4 Chronology

The chronology of growth increments was established using a reflected light image taken prior to sputter coating (Fig. 1d). Growth increments were defined as alternating light and dark bands, with each pair corresponding to one year of growth. The outermost growth increment was assigned to the year of sampling (2023), with each underlying increment subsequently assigned to the preceding year. To account for spatial heterogeneity in growth increment thickness across the transect, three evenly spaced measurements across its 180 µm width were averaged. Using this chronology and the coordinates in the stitched SEM image, each measured cell could be assigned to a specific year of formation. Growth increment thickness was then used to estimate the mean annual growth rate over the analysed interval. In addition, the number of cell rows contained within each growth increment was counted along the three measurement lines, and the mean was calculated.

2.5 Environmental data

Data on photosynthetically active radiation (PAR) at the sea surface (hereafter referred to as SSR) were obtained from NASA POWER using the R package *nasapower* (Sparks, 2018; version 4.2.5). The All-Sky Surface Total PAR [W/m^2] was downloaded at monthly resolution from 1984 to 2024 for the 1°×1° grid cell corresponding to Whangaparāoa Peninsula (36°35′56.05″ S 174°48′47.45″ E). These data are based on the methodology of Su et al. (2007), which defines PAR as the downwelling solar irradiance at the surface in the 400–700 nm range, including both direct and diffuse components.

Data on SST [°C] were obtained from the ERA5 reanalysis (Hersbach et al., 2020), which provides global data at 0.25°×0.25° spatial resolution. Monthly SST data were extracted for the period corresponding to the CCA record and the grid cell containing the sampling site, and subsequently converted to annual means.

Data on sea surface pCO_2 [µatm] were obtained from the dataset by Jersild et al. (2017; version 2023), using raw pCO_2 data with monthly resolution from 1982 to 2022 for the 1°×1° grid cell corresponding to the sampling site. These data are observation-based and interpolated using a two-step neural network, based on the methodology described in Landschützer et al. (2016).

2.6 Statistical analysis

Mean annual cell length and width, including standard errors of the mean, were calculated from the time-calibrated SEM measurements. Sub-annual variability was visualised using a rolling mean with a window width of 20 measurements (Fig. 3b, c), selected to balance noise reduction and preservation of sub-annual patterns, using the R package *zoo* (Zeileis and Grothendieck, 2005; version 1.8.14). While the SEM transect includes growth increments between 1984 and 2023, subsequent analyses were restricted to 1985–2022. The outermost increment (2023) was excluded because it represents an incomplete growth increment at the time of sampling in March. The innermost increment (1984) was excluded because it includes hypothallial tissue for which the onset of growth is unknown and which may integrate multiple years into a single increment.

https://doi.org/10.5194/egusphere-2026-2316
Preprint. Discussion started: 8 May 2026

Temporal trends in mean annual cell length, cell width, growth increment thickness and the number of cell rows per year were assessed using linear regression. To facilitate the comparison of datasets with different units and magnitudes, all variables, including the mean annual environmental variables SSR, SST and pCO_2, were standardised into dimensionless anomalies [(value - mean) / standard deviation]. Normality of these time series was assessed using Shapiro-Wilk tests. Because mean annual pCO_2 anomalies deviated from normality (Shapiro-Wilk test: $p = 0.015$), Spearman rank-order correlations were used to evaluate the individual relationships between mean annual cell length anomalies and all environmental anomalies.

Simple linear regression models were fitted to quantify the individual effects of each environmental variable on mean annual cell length anomalies. To separate interannual variability from long-term trends, linear models were used to detrend both cell length and environmental anomalies. The residuals were normally distributed, allowing analysis of relationships between detrended cell length and environmental anomalies using Pearson correlation tests.

Multiple linear regression was used to assess the independent contributions of mean annual SSR, SST and pCO_2 on mean annual cell length anomalies, while accounting for shared variance among predictors. Stepwise model selection based on Akaike's Information Criterion (AIC) was used to identify the most parsimonious combination of predictors. Temporal autocorrelation was assessed by inspecting the autocorrelation function (ACF) of model residuals for significant lag correlations.

Multicollinearity among predictors was assessed using pairwise correlation coefficients and Variance Inflation Factors (VIF) from the *car* package (Fox et al., 2024; version 3.1-3). VIF values for all predictors ranged from 1.41 to 2.05, well below commonly cited thresholds for multicollinearity concerns, such as VIF > 10 (Slinker and Glantz, 1985) or VIF > 5 (Sheather, 2009).

Finally, Pearson correlations were calculated between mean annual cell length anomalies and anomalies in growth increment thickness and the number of cell rows per year to explore controls on thallus growth. All statistical analyses were conducted in R (R Core Team, 2025; version 4.5.1).

3 Results

The analysed sample exhibits consistent cell orientation relative to the image plane across the measured transect. This is supported by truncated pit connections and the presence of closed cells, in which the cell lumen is not truncated and only the outer surface of the cell wall is visible (Fig. 2b, c). Substantial tilting would be expected to shift the apparent position of pit connections and cause closed cells to appear truncated along the transect.

The sampled protuberance exhibits a mean annual growth rate of 96.3 ± 3.5 µm between 1985 and 2022. A total of 3200 cells were measured along the transect between the epithallus and the top of the hypothallus, of which 2975 cells were retained after restricting the analysis to growth increments dated to 1985–2022. Mean annual cell length ranges from 10.1 ± 0.2 µm to 14.5 ± 0.2 µm and decreases significantly through time ($R^2_{adj} = 0.105$, $p = 0.027$; Fig. 4a), while the mean annual cell width ranges from 9.2 ± 0.1 µm to 11.2 ± 0.3 µm and shows no significant temporal trend ($R^2_{adj} = -0.019$, $p = 0.583$; Fig. 4b). Growth

https://doi.org/10.5194/egusphere-2026-2316
Preprint. Discussion started: 8 May 2026

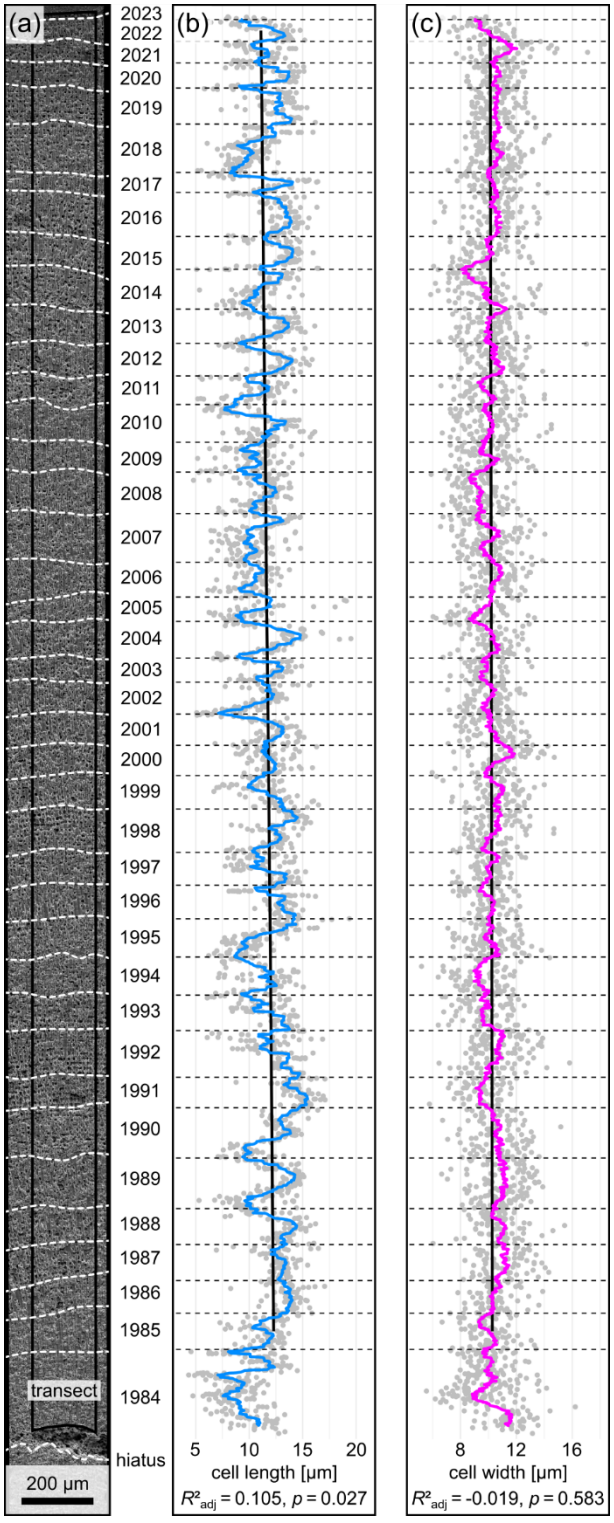

Figure 3. Stitched SEM image and cell measurements. **(a)** Stitched SEM image of the protuberance, extending approximately 4130 µm from the epithallus to the first hiatus (i.e. growth interruption). Annual growth boundaries, identified from a reflected light image of the specimen, are indicated by dotted white lines, and the box marks the transect encompassing all measured cells. **(b)** Cell length measurements of 2975 cells spanning 38 years (1985–2022), showing a significant decrease over time. The blue line represents a running mean (window width = 20), highlighting sub-annual variability. **(c)** Cell width measurements of the same cells show no significant temporal trend. The pink line represents a running mean (window width = 20).

increment thickness exhibits a slight but significant decrease (R^2_{adj} = 0.087, p = 0.040; Fig. 4c), while the number of cell rows per year shows no significant temporal trend (R^2_{adj} = 0.014, p = 0.225; Fig. 4d).

Figure 5 compares the time series of the dimensionless anomalies of mean annual cell length and the environmental variables, which include both interannual variability and the long-term trends. All anomaly time series were normally distributed (Shapiro-Wilk tests: p = 0.173–0.874), except for pCO_2 (Shapiro-Wilk test: p = 0.015), which deviated from normality. Spearman rank-order correlations showed a significant positive correlation between mean annual cell length and SSR anomalies (ρ = 0.49, p = 0.002), while no significant relationships were observed with SST (ρ = -0.13, p = 0.433) or pCO_2 anomalies (ρ = -0.32, p = 0.053). Simple linear regressions revealed a significant positive relationship between mean annual cell length and SSR anomalies (R^2_{adj} = 0.235, p = 0.001; Fig. 6a). SST anomalies showed no significant effect (R^2_{adj} = 0.005, p = 0.282; Fig. 6b), while pCO_2 anomalies exhibited a weak but significant negative relationship with cell length anomalies (R^2_{adj} = 0.101, p = 0.029; Fig. 6c).

https://doi.org/10.5194/egusphere-2026-2316
Preprint. Discussion started: 8 May 2026

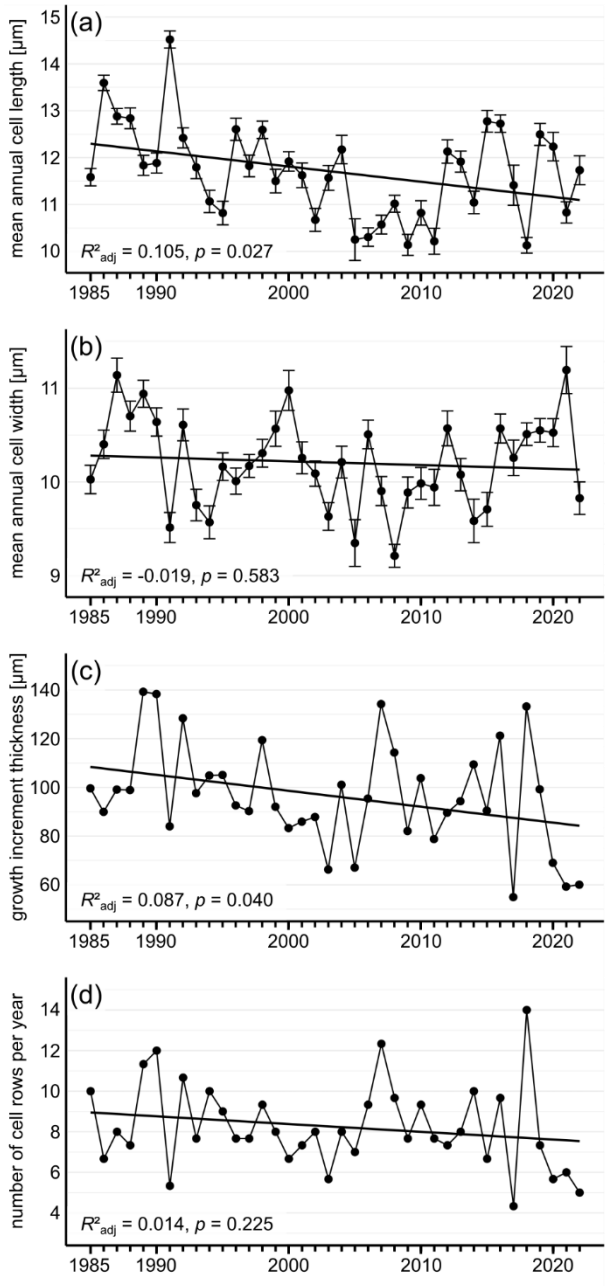

Detrending removed long-term trends in mean annual cell length and environmental variables, and all residuals were normally distributed (Shapiro-Wilk tests: p = 0.206–0.820). A positive correlation remained between detrended cell length and SSR anomalies (r = 0.41, p = 0.011), whereas no significant correlations were observed with detrended SST (r = 0.03, p = 0.880) or pCO_2 anomalies (r = 0.03, p = 0.874).

Multiple linear regression including mean annual SSR, SST and pCO_2 anomalies was performed to evaluate the independent contribution of each predictor to mean annual cell length anomalies (AIC = 103.89). Stepwise AIC model selection (Table 1) identified SSR anomalies as the strongest predictor of cell length anomalies (R^2_{adj} = 0.235, p = 0.001, AIC = 101.60). Inspection of the ACF indicated no significant temporal autocorrelation in model residuals. Despite a significant effect in the simple regression, pCO_2 anomalies were excluded from the most parsimonious AIC-selected model. Pairwise correlations among predictors were moderate ($r \leq 0.56$; Table 2) and VIF values were low (1.41–2.05), indicating no strong multicollinearity.

Pearson correlation analysis revealed a weak but significant negative relationship between cell length anomalies and the anomalies in the number of cell rows per year (r = -0.33, p = 0.045), whereas no significant correlation was found between cell length anomalies and growth increment thickness anomalies (r = 0.03, p = 0.864). In contrast, growth increment thickness anomalies and number of cell rows per year anomalies were strongly correlated (r = 0.91, p < 0.001).

Figure 4. Measured parameters of the carbonate skeleton from 1985 to 2022. **(a)** Mean annual cell length, showing a significant decrease over the study interval. **(b)** Mean annual cell width, showing no significant temporal trend. **(c)** Growth increment thickness, calculated as the mean of three measurements evenly spaced across the transect width. **(d)** Number of cell rows per year, calculated using the same approach. Lines indicate linear regressions, and error bars represent ± standard error of the mean

https://doi.org/10.5194/egusphere-2026-2316
Preprint. Discussion started: 8 May 2026

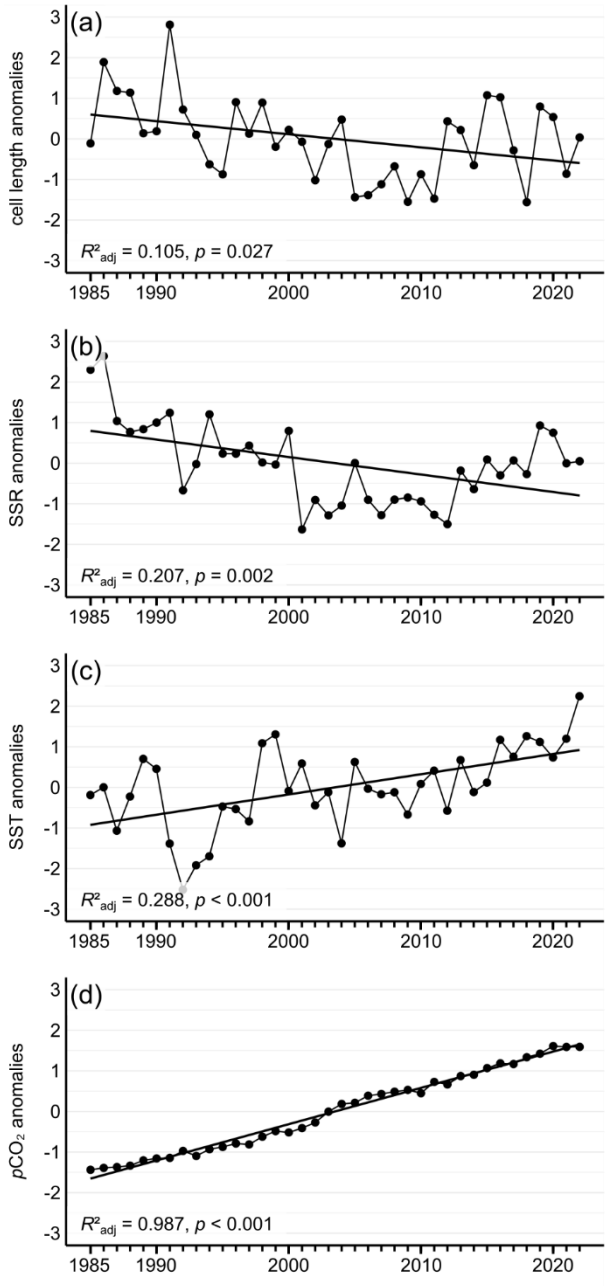

4 Discussion

Among the analysed environmental parameters, SSR is the strongest predictor of cell length in *S. nodosum*, whereas SST and pCO_2 explain comparatively little variance. Cell width remains largely stable over the 38-year record, indicating a limited sensitivity to environmental variability. This pattern aligns with observations by Bracchi et al. (2021), who reported a decrease in CCA cell length with water depth at the sampling sites, whereas cell width remained stable. Given the exponential attenuation of light with water depth (Kirk, 2011), these depth-related variations in cell length likely reflect differences in light availability. Conversely, Melbourne et al. (2023) documented an increase in cell lumen length and width between rhodoliths collected in the British Isles in the 1980s and 2014, primarily attributing these changes to long-term warming and acidification. In the present study, however, SSR rather than SST or pCO_2 emerges as the dominant driver of cell elongation, and detrended analysis indicates that this correlation reflects interannual variability rather than long-term trends. Although pCO_2 showed a significant effect on cell length in the simple linear model, this effect disappeared after detrending and was not retained in the AIC-selected model, suggesting that it does not exert a robust independent influence over the study period. This raises the possibility that the concurrent increase in SSR in the British Isles between 1977 and 2019 (Yuan et al., 2021) may also have contributed to the changes in cell dimensions reported by Melbourne et al. (2023).

Figure 5. Standardised anomalies of mean annual cell length and the mean annual environmental parameters from 1985 to 2022, calculated as (value - mean) / standard deviation. **(a)** Cell length anomalies, showing a significant decrease over the study interval. **(b)** SSR anomalies, showing a significant decrease. **(c)** SST anomalies, showing a significant increase. **(d)** pCO_2 anomalies, showing a significant increase. Lines indicate linear regressions.

https://doi.org/10.5194/egusphere-2026-2316
Preprint. Discussion started: 8 May 2026

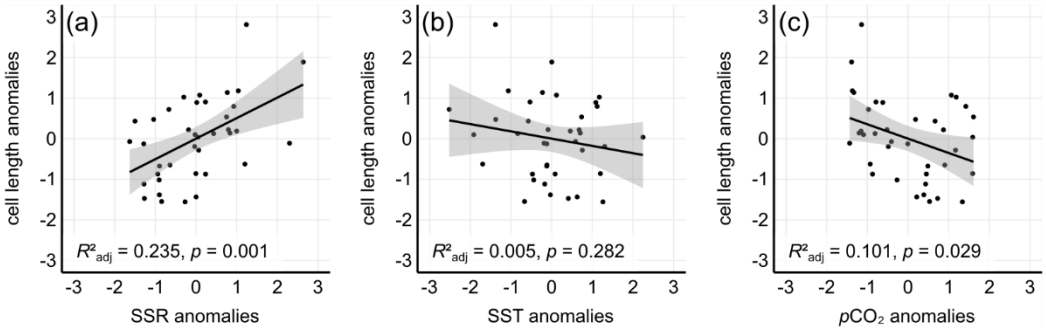

Figure 6. Linear relationships between mean annual cell length anomalies and environmental anomalies. **(a)** Significant positive correlation between cell length anomalies and SSR anomalies. **(b)** No significant correlation between cell length anomalies and SST anomalies. **(c)** Significant negative correlation between cell length anomalies and pCO_2 anomalies.

4.1 Environmental controls on cell elongation

The observed relationship between SSR and cell elongation in *S. nodosum* reflects the key influence of irradiance on photosynthetic activity (Burdett et al., 2014; Baek et al., 2022; Nguyen et al., 2022), growth rate (Adey, 1970; Halfar et al., 2011; Teichert and Freiwald, 2014) and carbonate production in coralline algae (Martin et al., 2013; Teichert and Freiwald, 2014; Krieger et al., 2023). As elevated irradiance enhances photosynthetic activity (Baek et al., 2022), it may promote cell elongation by increasing energy availability. However, irradiance exceeding species-specific thresholds can reduce photosynthetic efficiency (Burdett et al., 2014), and may constrain growth or cause thallus bleaching (Irving et al., 2004; Kang et al., 2024).

The apparent light dependence of cell elongation mirrors the light-controlled annual growth rates reported for some CCA taxa above a minimum temperature threshold (Adey, 1970; Williams et al., 2018). Adey (1970) demonstrated that the annual growth rate of *Clathromorphum* sp. is strongly temperature-controlled below approximately 4–5 °C, whereas light availability becomes the dominant control above this threshold. If cell elongation in *S. nodosum* responds to environmental drivers in a similarly threshold-dependent manner, the SSTs at Whangaparāoa Peninsula (long-term mean annual SST ≈ 17.3 ± 0.5 °C for 1985–2022 in the ERA5 data) likely exceed the range over which temperature limitation would be expected. This may explain the weak influence of SST on cell length observed in *S. nodosum*. Further studies across specimens from regions spanning broader SST gradients are needed to test the temperature-dependence of cell elongation.

While short-term laboratory experiments have shown that CCA increase cell dimensions and decrease cell wall thickness under elevated pCO_2 conditions (Ragazzola et al., 2012), longer-term experiments indicate they can acclimate within ten months, restoring their cell wall thickness to control levels (Ragazzola et al., 2013). Because these studies were conducted on *B. glaciale*, which belongs to a different taxonomic order than *S. nodosum*, direct comparisons should be made with caution. Nevertheless, *S. nodosum* may also acclimate over long timescales, potentially explaining the weak influence of pCO_2 on cell elongation.

https://doi.org/10.5194/egusphere-2026-2316
Preprint. Discussion started: 8 May 2026

While there was no significant relationship between cell length and growth increment thickness, a positive correlation between increment thickness and the number of cell rows per year indicates that annual thallus growth primarily reflects the production of new cell rows rather than variation in cell length.

Table 1. Results of the multiple linear regression of cell length anomalies on environmental predictor anomalies.

Overall model: AIC = 103.89 R^2_{adj} = 0.226 p = 0.008	AIC for omitting parameter	Estimate β	p value
SSR anomalies	109.72	0.48	0.009
SST anomalies	102.58	-0.15	0.436
pCO_2 anomalies	101.97	-0.06	0.789

4.2 Developmental controls on cell length and width

In contrast to cell length, cell width in *S. nodosum* remains largely stable over the 38-year record, showing neither a significant interannual trend nor pronounced intra-annual variability (Fig. 3b, c). This divergence likely reflects fundamental differences in the growth processes regulating cell length and width.

Cell elongation in CCA typically occurs gradually after the formation of a new cell in the intercalary meristem, with the mature length only reached between 3–10 cell rows below the meristem (Adey, 1964; Nash et al., 2019). This creates a temporal window during which SSR may influence the final cell length, likely by influencing energy availability for growth.

By contrast, the mature cell width is likely reached within the first row below the meristem (Adey, 1964), leaving considerably less time for environmental factors to exert an influence. Furthermore, the width of a newly formed cell appears to be developmentally constrained by the geometry of the underlying cell, as evidenced by the continuity of well-defined cell columns (Fig. 2c), leaving little scope for short-term variation in width. Consequently, both the rapid attainment of mature cell width and its structural dependence on pre-existing cell geometry likely account for the observed insensitivity to environmental variability.

Table 2. Correlation matrix used to assess multicollinearity among environmental predictor anomalies.

	SSR anomalies	SST anomalies	pCO_2 anomalies
SSR anomalies	1.00	0.00	-0.45
SST anomalies	0.00	1.00	0.56
pCO_2 anomalies	-0.45	0.56	1.00

https://doi.org/10.5194/egusphere-2026-2316
Preprint. Discussion started: 8 May 2026

4.3 Uncertainties affecting in situ light availability

Although interannual variations in SSR appear to be the strongest predictor of cell length among those investigated, they accounted for only ~23.5% of the observed variability, suggesting that additional environmental and biological factors also contribute to cell elongation.

Considerable uncertainties remain regarding the irradiance reaching the sampled rhodolith, as the SSR values based on Su et al. (2007) represent irradiance at the sea surface rather than in situ light levels, which may lead to an overestimation of light available to the specimen. Light reaching the seafloor is reduced by attenuation through the water column, which is not only affected by water depth but also by suspended sediments, phytoplankton biomass and coloured dissolved organic matter (Kirk, 2011). These components may be influenced by a wide range of drivers, such as storm events, land use and terrestrial runoff (Desmond et al., 2015; Pinkerton et al., 2022), and can give rise to abrupt episodic darkening events called "marine darkwaves" that persist from days to weeks and may reduce light availability by up to ~90% relative to long-term trends in shallow coastal waters of New Zealand (Thoral et al., 2026). In the Hauraki Gulf, suspended sediments are recognised as the primary driver of coastal turbidity, with the dominant factors varying across the estuarine–open coast gradient, including rainfall and tidal processes in sheltered environments and wave conditions at exposed coastal sites (Seers and Shears, 2015). Furthermore, shading by canopy-forming algae, such as kelp, can substantially reduce irradiance reaching the rhodolith (Figueiredo et al., 2000). These algae themselves may benefit from increasing SSR (Fortes and Lüning, 1980) and respond with faster growth, thereby partially offsetting the positive effects of higher SSR for the rhodolith. Although the water depth at the sampling location at Whangaparāoa Peninsula was only approximately 5 m, many rhodoliths were shaded by brown algae at the time of sampling (Fig. 1c). Because interannual variability in light attenuation and shading at the sampling site could not be quantified, the observed correlation between SSR and cell length likely underestimates the true influence of light availability on cell elongation.

Additionally, rhodoliths are unattached and may rotate due to wave action or bioturbation, altering the light exposure of individual protuberances or causing partial burial in sediments, which may damage tissues (Schlüter et al., 2021). Such rotations could contribute to variability in cell length, particularly if some areas face downwards more frequently than others, which can be linked to rhodolith morphology (Bosence, 1983). To better capture this heterogeneity, future studies should analyse protuberances along all three axes of collected rhodoliths.

4.4 Consequences for the rhodoliths and associated organisms

Finite element analysis by Ragazzola et al. (2012) demonstrated that an increase in cell dimensions, together with reduced cell wall thickness, increases total strain energy and produces an uneven internal stress distribution, thereby decreasing rhodolith structural integrity. As they are exposed to various mechanical stressors, such as grazing activity (Wisshak et al., 2019) and wave action (Melbourne et al., 2018), changes in structural integrity may affect their susceptibility to fragmentation. Increased

https://doi.org/10.5194/egusphere-2026-2316
Preprint. Discussion started: 8 May 2026

fragmentation could in turn reduce the habitat complexity provided by rhodoliths and consequently reduce local biodiversity (Teichert, 2014; Straube et al., 2024).

While declining SSR in New Zealand and the corresponding decrease in cell length observed in the specimen from Whangaparāoa Peninsula may enhance structural integrity, the direction and magnitude of SSR trends are spatially variable at the global scale (Yuan et al., 2021). As SSR is affected by aerosol concentration and cloud cover (Wild, 2016), a spatially heterogeneous pattern emerges (Yuan et al., 2021), potentially leading to localised shifts in cell length of varying magnitude among rhodolith-forming CCA.

Future studies should examine CCA across a broader range of environmental settings to assess how shifting light regimes influence their mechanical properties and role as ecosystem engineers. Although manual measurements of cell dimensions limited this study to a single protuberance, this approach provides an important step towards quantifying long-term variability in CCA cell dimensions. Implementing automated image analysis would enable more efficient sampling across multiple protuberances, allowing future studies to explore inter- and intraspecimen variability and improve the resolution of CCA cell dimension responses to environmental change.

5 Conclusion

This study provides a multi-decadal assessment of environmental controls on cell dimensions in *S. nodosum* and shows that SSR is a key driver of CCA cell length, whereas SST and pCO_2 exhibited no robust influences. Given that cell dimensions contribute to the structural integrity of rhodolith-forming CCA, variations in SSR may have direct implications for their role as ecosystem engineers. The spatial heterogeneity of SSR trends observed over recent decades suggests that these effects are likely region-specific, potentially leading to variable impacts on rhodoliths across different areas. Future research involving multiple specimens from diverse regions is essential to evaluate the broader applicability of these findings. Overall, these results highlight the central role of light availability in shaping rhodolith morphology and their ecological roles under changing environmental conditions.

Code and data availability

The data and code that support the findings of this study are openly available on Zenodo at https://doi.org/10.5281/zenodo.19694908.

https://doi.org/10.5194/egusphere-2026-2316
Preprint. Discussion started: 8 May 2026

Author contributions

Conceptualization: BS and ST; data curation: BS; formal analysis: BS; funding acquisition: TM and ST; sample collection: ST, TM, IP and WN; methodology: BS, ST and IP; supervision: ST; validation: BS, ST and IP; visualization: BS; writing – original draft: BS; writing – review & editing: BS, ST, IP, TM and WN.

Competing interests

The authors declare that they have no conflict of interest.

Acknowledgements

We thank Peter Marriott and Roberta D'Archino (Earth Sciences New Zealand), as well as Beau Masters and Ella Lis (School of Biological Sciences, University of Auckland), for their support during sample collection. We also thank Christian Schulbert (FAU Erlangen–Nürnberg) for technical support with the SEM, Ádám Kocsis (FAU Erlangen–Nürnberg) for statistical advice, and Kathryn Cryer and Birgit Leipner-Mata (FAU Erlangen–Nürnberg) for their assistance during sample preparation. Maria Lerich and Antonia Kaschmieder are acknowledged for testing the *Fiji*-based measurement workflow as part of their undergraduate thesis projects and for providing feedback that improved its application. AI tools were used for language editing and improving readability; all scientific content and interpretation remain the responsibility of the authors.

Financial support

This research was funded by the Deutsche Forschungsgemeinschaft (DFG, German Research Foundation) under grant number 453305163.

References

Adey, W. H.: The genus *Phymatolithon* in the Gulf of Maine, Hydrobiologia, 24, 377–420, https://doi.org/10.1007/BF00170412, 1964.

Adey, W. H.: The effects of light and temperature on growth rates in Boreal-Subarctic crustose corallines, J. Phycol., 6, 269–276, https://doi.org/10.1111/j.1529-8817.1970.tb02392.x, 1970.

Auer, G. and Piller, W. E.: Nanocrystals as phenotypic expression of genotypes - an example in coralline red algae, Sci. Adv., 6, eaay2126, https://doi.org/10.1126/sciadv.aay2126, 2020.

Baek, J.-W., Lee, J. S., Kim, S.-H., Lee, T., Jung, S. W., Lee, W.-C., Kim, K.-T., and An, S.-U.: Effects of Irradiance and Temperature on the Photosynthesis of the Crustose Coralline Algae *Pneophyllum fragile* (Corallinales, Rhodophyta) in the Coastal Waters of Korea, J. Mar. Sci. Eng., 10, 851, https://doi.org/10.3390/jmse10070851, 2022.

https://doi.org/10.5194/egusphere-2026-2316
Preprint. Discussion started: 8 May 2026

Basso, D.: Study of living calcareous algae by a paleontological approach: the non-geniculate Corallinaceae (Rhodophyta) of the soft bottoms of the Tyrrhenian Sea (western Mediterranean). The genera *Phymatolithon Foslie* and *Mesophyllum Lemoine*, Riv. It. Paleont. Strat., 100, 575–596, https://doi.org/10.13130/2039-4942/8602, 1994.

Basso, D., Fravega, P., and Vannuci, G.: The taxonomy of *Lithothamnium ramosissimum* (GÜMBEL non REUSS) CONTI and *Lithothamnium operculatum* (CONTI) CONTI (Rhodophyta, Corallinaceae), Facies, 37, 167–181, https://doi.org/10.1007/BF02537377, 1997.

Basso, D., Nalin, R., and Nelson, C. S.: Shallow-water *Sporolithon* rhodoliths from North Island (New Zealand), Palaios, 24, 92–103, https://doi.org/10.2110/palo.2008.p08-048r, 2009.

Borowitzka, M. A.: Calcification in aquatic plants, Plant Cell Environ., 7, 457–466, https://doi.org/10.1111/j.1365-3040.1984.tb01436.x, 1984.

Bosence, D. W. J.: The Occurrence and Ecology of Recent Rhodoliths — A Review, in: Coated Grains, edited by: Peryt, T. M., Springer, Berlin, Heidelberg, 225–242, https://doi.org/10.1007/978-3-642-68869-0_20, 1983.

Bracchi, V. A., Piazza, G., and Basso, D.: A stable ultrastructural pattern despite variable cell size in *Lithothamnion corallioides*, Biogeosciences, 18, 6061–6076, https://doi.org/10.5194/bg-18-6061-2021, 2021.

Burdett, H. L., Kamenos, N. A., and Law, A.: Using coralline algae to understand historic marine cloud cover, Palaeogeogr. Palaeoclimatol. Palaeoecol., 302, 65–70, https://doi.org/10.1016/j.palaeo.2010.07.027, 2011.

Burdett, H. L., Keddie, V., MacArthur, N., McDowall, L., McLeish, J., Spielvogel, E., Hatton, A. D., and Kamenos, N. A.: Dynamic photoinhibition exhibited by red coralline algae in the Red Sea, BMC Plant Biol., 14, 139, https://doi.org/10.1186/1471-2229-14-139, 2014.

Cabioch, J. and Giraud, G.: Structural aspects of biomineralization in the coralline algae (calcified Rhodophyceae), in: Biomineralization in lower plants and animals, edited by: Leadbeater, B. S. C. and Riding, R., Clarendon Press, Oxford, 141–156, 1986.

Cabrito, A., de Juan, S., Hinz, H., and Maynou, F.: Morphological insights into the three-dimensional complexity of rhodolith beds, Mar. Biol., 171, 127, https://doi.org/10.1007/s00227-024-04437-y, 2024.

Caragnano, A., Basso, D., and Rodondi, G.: Growth rates and ecology of coralline rhodoliths from the Ras Ghamila back reef lagoon, Red Sea, Mar. Ecol., 37, 713–726, https://doi.org/10.1111/maec.12371, 2016.

Caragnano, A., Basso, D., Storz, D., Jacob, D. E., Ragazzola, F., Benzoni, F., and Dutrieux, E.: Elemental variability in the coralline alga *Lithophyllum yemenense* as an archive of past climate in the Gulf of Aden (NW Indian Ocean), J. Phycol., 53, 381–395, https://doi.org/10.1111/jpy.12509, 2017.

de Carvalho, R. T., Salgado, L. T., Amado Filho, G. M., Leal, R. N., Werckmann, J., Rossi, A. L., Campos, A. P. C., Karez, C. S., and Farina, M.: Biomineralization of calcium carbonate in the cell wall of *Lithothamnion crispatum* (Hapalidiales, Rhodophyta): correlation between the organic matrix and the mineral phase, J. Phycol., 53, 642–651, https://doi.org/10.1111/jpy.12526, 2017.

Chan, P., Halfar, J., Adey, W., Hetzinger, S., Zack, T., Moore, G. W. K., Wortmann, U. G., Williams, B., and Hou, A.: Multicentennial record of Labrador Sea primary productivity and sea-ice variability archived in coralline algal barium, Nat. Commun., 8, 15543, https://doi.org/10.1038/ncomms15543, 2017.

https://doi.org/10.5194/egusphere-2026-2316
Preprint. Discussion started: 8 May 2026

Cornwall, C. E., Carlot, J., Branson, O., Courtney, T. A., Harvey, B. P., Perry, C. T., Andersson, A. J., Diaz-Pulido, G., Johnson, M. D., Kennedy, E., Krieger, E. C., Mallela, J., McCoy, S. J., Nugues, M. M., Quinter, E., Ross, C. L., Ryan, E., Saderne, V., and Comeau, S.: Crustose coralline algae can contribute more than corals to coral reef carbonate production, Commun. Earth Environ., 4, 105, https://doi.org/10.1038/s43247-023-00766-w, 2023.

Darrenougue, N., De Deckker, P., Eggins, S., and Payri, C.: Sea-surface temperature reconstruction from trace elements variations of tropical coralline red algae, Quat. Sci. Rev., 93, 34–46, https://doi.org/10.1016/j.quascirev.2014.03.005, 2014.

Darrenougue, N., De Deckker, P., Eggins, S., Fallon, S., and Payri, C.: A record of mining and industrial activities in New Caledonia based on trace elements in rhodolith-forming coralline red algae, Chem. Geol., 493, 24–36, https://doi.org/10.1016/j.chemgeo.2018.05.014, 2018.

Desmond, M. J., Pritchard, D. W., and Hepburn, C. D.: Light Limitation within Southern New Zealand Kelp Forest Communities, PLOS ONE, 10, e0123676, https://doi.org/10.1371/journal.pone.0123676, 2015.

Fietzke, J., Ragazzola, F., Halfar, J., Dietze, H., Foster, L. C., Hansteen, T. H., Eisenhauer, A., and Steneck, R. S.: Century-scale trends and seasonality in pH and temperature for shallow zones of the Bering Sea, Proc. Natl. Acad. Sci. USA, 112, 2960–2965, https://doi.org/10.1073/pnas.1419216112, 2015.

Figueiredo, M. A. de O., Kain (Jones), J. M., and Norton, T. A.: Responses of crustose corallines to epiphyte and canopy cover, J. Phycol., 36, 17–24, https://doi.org/10.1046/j.1529-8817.2000.98208.x, 2000.

Fortes, M. D. and Lüning, K.: Growth rates of North Sea macroalgae in relation to temperature, irradiance and photoperiod, Helgol. Meeresunters., 34, 15–29, https://doi.org/10.1007/BF01983538, 1980.

Fox, J., Weisberg, S., Price, B., Adler, D., Bates, D., Baud-Bovy, G., Bolker, B., Ellison, S., Firth, D., Friendly, M., Gorjanc, G., Graves, S., Heiberger, R., Krivitsky, P., Laboissiere, R., Maechler, M., Monette, G., Murdoch, D., Nilsson, H., Ogle, D., Ripley, B., Short, T., Venables, W., Walker, S., Winsemius, D., Zeileis, A., and R-Core: car: Companion to Applied Regression, CRAN [code], https://doi.org/10.32614/CRAN.package.car, 2024.

Freiwald, A. and Henrich, R.: Reefal coralline algal build-ups within the Arctic Circle: morphology and sedimentary dynamics under extreme environmental seasonality, Sedimentology, 41, 963–984, https://doi.org/10.1111/j.1365-3091.1994.tb01435.x, 1994.

Gabsteiger, M., Pyko, I., Wisshak, M., and Teichert, S.: Quantifying floridean starch storage patterns in Arctic rhodoliths: blue carbon implications, Polar Res., 44, 10992, https://doi.org/10.33265/polar.v44.10992, 2025.

Gamboa, G., Halfar, J., Hetzinger, S., Adey, W., Zack, T., Kunz, B., and Jacob, D. E.: Mg/Ca ratios in coralline algae record northwest Atlantic temperature variations and North Atlantic Oscillation relationships, J. Geophys. Res. Oceans, 115, https://doi.org/10.1029/2010JC006262, 2010.

Granier, B.: On the fossil alga *Elianella elegans* Pfender & Basse, 1948, and its so-called lookalikes, with description of *Elianella brasiliana* n.sp Revision of the Juliette Pfender Collection. Part 1, Carnets de Geologie, 16, 213–229, https://doi.org/10.4267/2042/59920, 2016.

Halfar, J., Zack, T., Kronz, A., and Zachos, J. C.: Growth and high-resolution paleoenvironmental signals of rhodoliths (coralline red algae): A new biogenic archive, J. Geophys. Res. Oceans, 105, 22107–22116, https://doi.org/10.1029/1999JC000128, 2000.

https://doi.org/10.5194/egusphere-2026-2316
Preprint. Discussion started: 8 May 2026

Halfar, J., Steneck, R. S., Joachimski, M., Kronz, A., and Wanamaker, A. D. Jr.: Coralline red algae as high-resolution climate recorders, Geology, 36, 463–466, https://doi.org/10.1130/G24635A.1, 2008.

Halfar, J., Williams, B., Hetzinger, S., Steneck, R. S., Lebednik, P., Winsborough, C., Omar, A., Chan, P., and Wanamaker, A. D.: 225 years of Bering Sea climate and ecosystem dynamics revealed by coralline algal growth-increment widths, Geology, 39, 579–582, https://doi.org/10.1130/G31996.1, 2011.

Halfar, J., Adey, W. H., Kronz, A., Hetzinger, S., Edinger, E., and Fitzhugh, W. W.: Arctic sea-ice decline archived by multicentury annual-resolution record from crustose coralline algal proxy, Proc. Natl. Acad. Sci. USA, 110, 19737–19741, https://doi.org/10.1073/pnas.1313775110, 2013.

Hersbach, H., Bell, B., Berrisford, P., Hirahara, S., Horányi, A., Muñoz-Sabater, J., Nicolas, J., Peubey, C., Radu, R., Schepers, D., Simmons, A., Soci, C., Abdalla, S., Abellan, X., Balsamo, G., Bechtold, P., Biavati, G., Bidlot, J., Bonavita, M., De Chiara, G., Dahlgren, P., Dee, D., Diamantakis, M., Dragani, R., Flemming, J., Forbes, R., Fuentes, M., Geer, A., Haimberger, L., Healy, S., Hogan, R. J., Hólm, E., Janisková, M., Keeley, S., Laloyaux, P., Lopez, P., Lupu, C., Radnoti, G., de Rosnay, P., Rozum, I., Vamborg, F., Villaume, S., and Thépaut, J.-N.: The ERA5 global reanalysis, Q. J. R. Meteorol. Soc., 146, 1999–2049, https://doi.org/10.1002/qj.3803, 2020.

Hetzinger, S., Halfar, J., Kronz, A., Steneck, R. S., Adey, W., Lebednik, P., and Schöne, B.: High-resolution Mg/Ca ratios in a coralline red alga as a proxy for Bering Sea temperature variations from 1902 to 1967, Palaios, 24, 406–412, https://doi.org/10.2110/palo.2008.p08-116r, 2009.

Hetzinger, S., Halfar, J., Zajacz, Z., and Wisshak, M.: Early start of 20th-century Arctic sea-ice decline recorded in Svalbard coralline algae, Geology, 47, 963–967, https://doi.org/10.1130/G46507.1, 2019.

Irvine, L. M. and Chamberlain, Y. M.: Seaweeds of the British Isles, vol. 1. Rhodophyta, Part 2B Corallinales, Hildenbrandiales, HMSO, London, 276 pp., 1994.

Irving, A. D., Connell, S. D., and Elsdon, T. S.: Effects of kelp canopies on bleaching and photosynthetic activity of encrusting coralline algae, J. Exp. Mar. Biol. Ecol., 310, 1–12, https://doi.org/10.1016/j.jembe.2004.03.020, 2004.

Jersild, A., Landschützer, P., Gruber, N., and Bakker, D. C. E.: An observation-based global monthly gridded sea surface pCO2 and air-sea CO2 flux product from 1982 onward and its monthly climatology (NCEI Accession 0160558), NOAA National Centers for Environmental Information (NCEI) [data set], https://doi.org/10.7289/v5z899n6, 2017.

Kamenos, N. A. and Law, A.: Temperature Controls on Coralline Algal Skeletal Growth, J. Phycol., 46, 331–335, https://doi.org/10.1111/j.1529-8817.2009.00780.x, 2010.

Kamenos, N. A., Cusack, M., and Moore, P. G.: Coralline algae are global palaeothermometers with bi-weekly resolution, Geochim. Cosmochim. Acta, 72, 771–779, https://doi.org/10.1016/j.gca.2007.11.019, 2008.

Kang, E. J., Kim, Y. R., Lee, H. W., Kim, H., Kim, Y. S., and Kim, J.-H.: Effect of light intensity on photophysiology and growth dynamics of crustose coralline algae (CCA): implications for the loss of canopy-forming algae, Hydrobiologia, 851, 4341–4352, https://doi.org/10.1007/s10750-024-05553-y, 2024.

Kim, G. H., Nagasato, C., Kwak, M., Lee, J. W., Hong, C. Y., Klochkova, T. A., and Motomura, T.: Intercellular transport across pit-connections in the filamentous red alga *Griffithsia monilis*, Algae, 37, 75–84, https://doi.org/10.4490/algae.2022.37.2.16, 2022.

https://doi.org/10.5194/egusphere-2026-2316
Preprint. Discussion started: 8 May 2026

Kirk, J. T. O.: Light and Photosynthesis in Aquatic Ecosystems, 3rd ed., Cambridge University Press, Cambridge, 649 pp., 2011.

Krieger, E. C., Nelson, W. A., Grand, J., Le Ru, E. C., Bury, S. J., Cossais, A., Davy, S. K., and Cornwall, C. E.: The role of irradiance in controlling coralline algal calcification, Limnol. Oceanogr., 68, 1269–1284, https://doi.org/10.1002/lno.12345, 2023.

Landschützer, P., Gruber, N., and Bakker, D. C. E.: Decadal variations and trends of the global ocean carbon sink, Glob. Biogeochem. Cycles, 30, 1396–1417, https://doi.org/10.1002/2015GB005359, 2016.

Leclerc, N., Halfar, J., Hetzinger, S., Tsay, A., and Moore, G. W. K.: Growth Increments of Coralline Red Alga *Clathromorphum Compactum* Capture Sea-Ice Variability Links to Arctic and Atlantic Multidecadal Oscillations (1805–2015), Geophys. Res. Lett., 51, e2023GL105914, https://doi.org/10.1029/2023GL105914, 2024.

Littler, M. M., Littler, D. S., Blair, S. M., and Norris, J. N.: Deepest Known Plant Life Discovered on an Uncharted Seamount, Science, 227, 57–59, https://doi.org/10.1126/science.227.4682.57, 1985.

López Correa, M., Teichert, S., Ragazzola, F., Cazorla Vázquez, S., Engel, F. B., Hurle, K., Mazzoli, C., Kuklinski, P., Raiteri, G., and Lombardi, C.: Structural and Geochemical Assessment of the Coralline Alga *Tethysphytum antarcticum* from Terra Nova Bay, Ross Sea, Antarctica, Minerals, 13, 215, https://doi.org/10.3390/min13020215, 2023.

Martin, S., Charnoz, A., and Gattuso, J.-P.: Photosynthesis, respiration and calcification in the Mediterranean crustose coralline alga *Lithophyllum cabiochae* (Corallinales, Rhodophyta), Eur. J. Phycol., 48, 163–172, https://doi.org/10.1080/09670262.2013.786790, 2013.

McCoy, S. J., Pueschel, C. M., Cornwall, C. E., Comeau, S., Kranz, S. A., Spindel, N. B., and Borowitzka, M. A.: Calcification in the coralline red algae: a synthesis, Phycologia, 62, 648–666, https://doi.org/10.1080/00318884.2023.2285673, 2023.

Melbourne, L. A., Denny, M. W., Harniman, R. L., Rayfield, E. J., and Schmidt, D. N.: The importance of wave exposure on the structural integrity of rhodoliths, J. Exp. Mar. Biol. Ecol., 503, 109–119, https://doi.org/10.1016/j.jembe.2017.11.007, 2018.

Melbourne, L. A., Brodie, J., Rayfield, E. J., Titelboim, D., Lord, O. T., and Schmidt, D. N.: Environmental impacts on the structural integrity of British rhodoliths, Sci. Rep., 13, 13473, https://doi.org/10.1038/s41598-023-40292-5, 2023.

Nash, M. C., Diaz-Pulido, G., Harvey, A. S., and Adey, W.: Coralline algal calcification: A morphological and process-based understanding, PLoS One, 14, e0221396, https://doi.org/10.1371/journal.pone.0221396, 2019.

Nguyen, H. T. T., Pritchard, D. W., Desmond, M. J., and Hepburn, C. D.: Coralline photosynthetic physiology across a steep light gradient, Photosynth. Res., 153, 43–57, https://doi.org/10.1007/s11120-022-00899-7, 2022.

Pinkerton, M., Gall, M., O'Callaghan, J., Thoral, F., and Swales, A.: Monitoring coastal suspended sediment in Aotearoa New Zealand: utility of satellite remote sensing, NIWA Client Report, NIWA Project: DOC21305, 112 pp., https://doi.org/10.13140/RG.2.2.13171.60962, 2022.

Preibisch, S., Saalfeld, S., and Tomancak, P.: Globally optimal stitching of tiled 3D microscopic image acquisitions, Bioinformatics, 25, 1463–1465, https://doi.org/10.1093/bioinformatics/btp184, 2009.

Pueschel, C. M.: Formation of secondary pit connections by conjunctor cells in a coralline red alga, Phycologia, 60, 644–652, https://doi.org/10.1080/00318884.2021.1986662, 2021.

https://doi.org/10.5194/egusphere-2026-2316
Preprint. Discussion started: 8 May 2026

Pyko, I., Wisshak, M., and Teichert, S.: Depth-Related Controls on the Quantitative Composition of Rhodolith Matrices in the High Arctic, Aquat. Conserv.: Mar. Freshw. Ecosyst., 35, e70045, https://doi.org/10.1002/aqc.70045, 2025.

R Core Team: R: A Language and Environment for Statistical Computing, R Foundation for Statistical Computing, Vienna, Austria, https://www.R-project.org/, 2025.

Ragazzola, F., Foster, L. C., Form, A., Anderson, P. S. L., Hansteen, T. H., and Fietzke, J.: Ocean acidification weakens the structural integrity of coralline algae, Glob. Change Biol., 18, 2804–2812, https://doi.org/10.1111/j.1365-2486.2012.02756.x, 2012.

Ragazzola, F., Foster, L. C., Form, A. U., Büscher, J., Hansteen, T. H., and Fietzke, J.: Phenotypic plasticity of coralline algae in a High CO2 world, Ecol. Evol., 3, 3436–3446, https://doi.org/10.1002/ece3.723, 2013.

Ragazzola, F., Foster, L. C., Jones, C. J., Scott, T. B., Fietzke, J., Kilburn, M. R., and Schmidt, D. N.: Impact of high CO2 on the geochemistry of the coralline algae *Lithothamnion glaciale*, Sci. Rep., 6, 20572, https://doi.org/10.1038/srep20572, 2016.

Ragazzola, F., Kolzenburg, R., Zekonyte, J., Teichert, S., Jiang, C., Žuljević, A., Caragnano, A., and Falace, A.: Structural and Elemental Analysis of the Freshwater, Low-Mg Calcite Coralline Alga *Pneophyllum cetinaensis*, Plants, 9, 1089, https://doi.org/10.3390/plants9091089, 2020.

Rebelo, A. C., Teichert, S., Bracchi, V. A., Rasser, M. W., and Basso, D.: Editorial: Crustose coralline red algae frameworks and rhodoliths: Past and present, Front. Earth Sci., 10, 1090091, https://doi.org/10.3389/feart.2022.1090091, 2022.

Schindelin, J., Arganda-Carreras, I., Frise, E., Kaynig, V., Longair, M., Pietzsch, T., Preibisch, S., Rueden, C., Saalfeld, S., Schmid, B., Tinevez, J.-Y., White, D. J., Hartenstein, V., Eliceiri, K., Tomancak, P., and Cardona, A.: Fiji: an open-source platform for biological-image analysis, Nat. Methods, 9, 676–682, https://doi.org/10.1038/nmeth.2019, 2012.

Schlüter, M., Pyko, I., Wisshak, M., Schulbert, C., and Teichert, S.: Growth Interruptions in Arctic Rhodoliths Correspond to Water Depth and Rhodolith Morphology, Minerals, 11, 538, https://doi.org/10.3390/min11050538, 2021.

Schubert, N., Tuya, F., Peña, V., Horta, P. A., Salazar, V. W., Neves, P., Ribeiro, C., Otero-Ferrer, F., Espino, F., Schoenrock, K., Ragazzola, F., Olivé, I., Giaccone, T., Nannini, M., Mangano, M. C., Sará, G., Mancuso, F. P., Tantillo, M. F., Bosch-Belmar, M., Martin, S., Le Gall, L., Santos, R., and Silva, J.: "Pink power"—the importance of coralline algal beds in the oceanic carbon cycle, Nat. Commun., 15, 8282, https://doi.org/10.1038/s41467-024-52697-5, 2024.

Seers, B. M. and Shears, N. T.: Spatio-temporal patterns in coastal turbidity - Long-term trends and drivers of variation across an estuarine-open coast gradient, Estuar. Coast. Shelf Sci., 154, 137–151, https://doi.org/10.1016/j.ecss.2014.12.018, 2015.

Sheather, S.: A Modern Approach to Regression with R, Springer, New York, 398 pp., 2009.

Sletten, H. R., Gillikin, D. P., Halfar, J., Andrus, C. F. T., and Guzmán, H. M.: Skeletal growth controls on Mg/Ca and P/Ca ratios in tropical Eastern Pacific rhodoliths (coralline red algae), Chem. Geol., 465, 1–10, https://doi.org/10.1016/j.chemgeo.2017.05.010, 2017.

Slinker, B. K. and Glantz, S. A.: Multiple regression for physiological data analysis: the problem of multicollinearity, Am. J. Physiol., 249, R1–R12, https://doi.org/10.1152/ajpregu.1985.249.1.R1, 1985.

Smith, A. M., Sutherland, J. E., Kregting, L., Farr, T. J., and Winter, D. J.: Phylomineralogy of the Coralline red algae: Correlation of skeletal mineralogy with molecular phylogeny, Phytochemistry, 81, 97–108, https://doi.org/10.1016/j.phytochem.2012.06.003, 2012.

https://doi.org/10.5194/egusphere-2026-2316
Preprint. Discussion started: 8 May 2026

Sparks, A.: nasapower: A NASA POWER Global Meteorology, Surface Solar Energy and Climatology Data Client for R, CRAN [code], https://doi.org/10.32614/CRAN.package.nasapower, 2018.

Straube, E., Neumann, H., Wisshak, M., Mathes, G., and Teichert, S.: Bayesian analysis of biodiversity patterns via beam trawl versus video transect—a comparative case study of Svalbard rhodolith beds, Biodivers. Conserv., 33, 1099–1123, https://doi.org/10.1007/s10531-024-02788-y, 2024.

Su, W., Charlock, T. P., Rose, F. G., and Rutan, D.: Photosynthetically active radiation from Clouds and the Earth's Radiant Energy System (CERES) products, J. Geophys. Res. Biogeosci., 112, https://doi.org/10.1029/2006JG000290, 2007.

Teichert, S.: Rhodoliths (Corallinales, Rhodophyta) as a biosedimentary system in Arctic Environments (Svalbard Archipelago, Norway), Ph.D. thesis, Dept. of Geography and Earth Sciences, Friedrich-Alexander-Universität Erlangen-Nürnberg, Erlangen, 2013.

Teichert, S.: Hollow rhodoliths increase Svalbard's shelf biodiversity, Sci. Rep., 4, https://doi.org/10.1038/srep06972, 2014.

Teichert, S.: Attached and free-living crustose coralline algae and their functional traits in the geological record and today, Facies, 70, 8, https://doi.org/10.1007/s10347-024-00682-1, 2024.

Teichert, S. and Freiwald, A.: Polar coralline algal $CaCO_3$-production rates correspond to intensity and duration of the solar radiation, Biogeosciences, 11, 833–842, https://doi.org/10.5194/bg-11-833-2014, 2014.

Teichert, S., Woelkerling, W., and Munnecke, A.: Coralline red algae from the Silurian of Gotland indicate that the order Corallinales (Corallinophycidae, Rhodophyta) is much older than previously thought, Palaeontology, 62, 599–613, https://doi.org/10.1111/pala.12418, 2019.

Teichert, S., Steinbauer, M., and Kiessling, W.: A possible link between coral reef success, crustose coralline algae and the evolution of herbivory, Sci. Rep., 10, 17748, https://doi.org/10.1038/s41598-020-73900-9, 2020a.

Teichert, S., Voigt, N., and Wisshak, M.: Do skeletal Mg/Ca ratios of Arctic rhodoliths reflect atmospheric CO2 concentrations?, Polar Biol., 43, 2059–2069, https://doi.org/10.1007/s00300-020-02767-3, 2020b.

Teichert, S., Reddin, C. J., and Wisshak, M.: In situ decrease in rhodolith growth associated with Arctic climate change, Glob. Change Biol., 30, e17300, https://doi.org/10.1111/gcb.17300, 2024.

Thoral, F., Pinkerton, M. H., Montie, S., Thomsen, M. S., Battershill, C. N., Filbee-Dexter, K., Gall, M., Miller, R. J., Orchard, S., Reed, D. C., Tait, L. W., Virgin, S. D. S., Wernberg, T., Zeldis, J., and Schiel, D. R.: Marine darkwave as an event-based framework to assess unusual periods of reduced underwater light availability, Commun. Earth Environ., 7, 4, https://doi.org/10.1038/s43247-025-03023-4, 2026.

Vesk, M. and Borowitzka, M. A.: Ultrastructure of Tetrasporogenesis in the Coralline Alga *Haliptilon cuvieri* (Rhodophyta), J. Phycol., 20, 501–515, https://doi.org/10.1111/j.0022-3646.1984.00501.x, 1984.

Wild, M.: Decadal changes in radiative fluxes at land and ocean surfaces and their relevance for global warming, WIREs Clim. Change, 7, 91–107, https://doi.org/10.1002/wcc.372, 2016.

Williams, B., Halfar, J., DeLong, K. L., Hetzinger, S., Steneck, R. S., and Jacob, D. E.: Multi-specimen and multi-site calibration of Aleutian coralline algal Mg/Ca to sea surface temperature, Geochim. Cosmochim. Acta, 139, 190–204, https://doi.org/10.1016/j.gca.2014.04.006, 2014.

https://doi.org/10.5194/egusphere-2026-2316
Preprint. Discussion started: 8 May 2026

Williams, S., Adey, W., Halfar, J., Kronz, A., Gagnon, P., Bélanger, D., and Nash, M.: Effects of light and temperature on Mg uptake, growth, and calcification in the proxy climate archive *Clathromorphum compactum*, Biogeosciences, 15, 5745–5759, https://doi.org/10.5194/bg-15-5745-2018, 2018.

Wilson, S., Blake, C., Berges, J. A., and Maggs, C. A.: Environmental tolerances of free-living coralline algae (maerl): implications for European marine conservation, Biol. Conserv., 120, 279–289, https://doi.org/10.1016/j.biocon.2004.03.001, 2004.

Wisshak, M., Bartholomä, A., Beuck, L., Büscher, J., Form, A., Freiwald, A., Halfar, J., Hetzinger, S., van Heugten, B., Hissmann, K., Holler, P., Meyer, N., Neumann, H., Raddatz, J., Rüggeberg, A., Teichert, S., and Wehrmann, A.: Habitat characteristics and carbonate cycling of macrophyte-supported polar carbonate factories (Svalbard) - Cruise No. MSM55 - June 11 - June 29, 2016 - Reykjavik (Iceland) - Longyearbyen (Norway), MARUM – Center for Marine Environmental Sciences, University of Bremen, Bremen, 58 pp., https://doi.org/10.2312/cr_msm55, 2017.

Wisshak, M., Neumann, H., Rüggeberg, A., Büscher, J. V., Linke, P., and Raddatz, J.: Epibenthos Dynamics and Environmental Fluctuations in Two Contrasting Polar Carbonate Factories (Mosselbukta and Bjørnøy-Banken, Svalbard), Front. Mar. Sci., 6, https://doi.org/10.3389/fmars.2019.00667, 2019.

Woelkerling, W. J.: The coralline red algae. An analysis of the genera and subfamilies of the nongeniculate Corallinaceae, Oxford University Press, Oxford, 280 pp., 1988.

Yuan, M., Leirvik, T., and Wild, M.: Global Trends in Downward Surface Solar Radiation from Spatial Interpolated Ground Observations during 1961–2019, J. Clim., 34, 9501–9521, https://doi.org/10.1175/JCLI-D-21-0165.1, 2021.

Zeileis, A. and Grothendieck, G.: zoo: S3 Infrastructure for Regular and Irregular Time Series, CRAN [code], https://doi.org/10.32614/CRAN.package.zoo, 2005.

Žuljević, A., Kaleb, S., Peña, V., Despalatović, M., Cvitković, I., De Clerck, O., Le Gall, L., Falace, A., Vita, F., Braga, J. C., and Antolić, B.: First freshwater coralline alga and the role of local features in a major biome transition, Sci. Rep., 6, 19642, https://doi.org/10.1038/srep19642, 2016.